

12-2018

An Assessment of Computational Methods for Calculating Accurate Structures and Energies of Bio-Relevant Polysulfur/Selenium-Containing Compounds


Sahar Nikoo
University of Windsor

Paul Meister
University of Windsor

John Hayward
University of Windsor

James Gauld
University of Windsor

Follow this and additional works at: <https://scholar.uwindsor.ca/chemistrybiochemistrypub>

 Part of the [Biochemistry, Biophysics, and Structural Biology Commons](#), and the [Chemistry Commons](#)

Recommended Citation

Nikoo, Sahar; Meister, Paul; Hayward, John; and Gauld, James. (2018). An Assessment of Computational Methods for Calculating Accurate Structures and Energies of Bio-Relevant Polysulfur/Selenium-Containing Compounds. *Molecules*, 23 (12), 3323.
<https://scholar.uwindsor.ca/chemistrybiochemistrypub/97>

This Article is brought to you for free and open access by the Department of Chemistry and Biochemistry at Scholarship at UWindsor. It has been accepted for inclusion in Chemistry and Biochemistry Publications by an authorized administrator of Scholarship at UWindsor. For more information, please contact scholarship@uwindsor.ca.

Article

An Assessment of Computational Methods for Calculating Accurate Structures and Energies of Bio-Relevant Polysulfur/Selenium-Containing Compounds

Sahar Nikoo [†], Paul J. Meister [†] , John J. Hayward and James W. Gauld ^{*} 

Department of Chemistry and Biochemistry, University of Windsor, Windsor, ON N9B 3P4, Canada; nikoo@uwindsor.ca (S.N.); meisterp@uwindsor.ca (P.J.M.); jhayward@uwindsor.ca (J.J.H.)

* Correspondence: gauld@uwindsor.ca; Tel.: +1-519-253-3000 (ext. 3992); Fax: +1-519-973-7098

[†] These authors contributed equally.

Received: 27 November 2018; Accepted: 12 December 2018; Published: 14 December 2018



Abstract: The heavier chalcogens sulfur and selenium are important in organic and inorganic chemistry, and the role of such chalcogens in biological systems has recently gained more attention. Sulfur and, to a lesser extent selenium, are involved in diverse reactions from redox signaling to antioxidant activity and are considered essential nutrients. We investigated the ability of the DFT functionals (B3LYP, B3PW91, ω B97XD, M06-2X, and M08-HX) relative to electron correlation methods MP2 and QCISD to produce reliable and accurate structures as well as thermochemical data for sulfur/selenium-containing systems. Bond lengths, proton affinities (PA), gas phase basicities (GPB), chalcogen–chalcogen bond dissociation enthalpies (BDE), and the hydrogen affinities (HA) of thiy1/selenyl radicals were evaluated for a range of small polysulfur/selenium compounds and cysteine per/polysulfide. The S–S bond length was found to be the most sensitive to basis set choice, while the geometry of selenium-containing compounds was less sensitive to basis set. In mixed chalcogens species of sulfur and selenium, the location of the sulfur atom affects the S–Se bond length as it can hold more negative charge. PA, GPB, BDE, and HA of selenium systems were all lower, indicating more acidity and more stability of radicals. Extending the sulfur chain in cysteine results in a decrease of BDE and HA, but these plateau at a certain point (199 kJ mol^{-1} and 295 kJ mol^{-1}), and PA and GPB are also decreased relative to the thiol, indicating that the polysulfur species exist as thiolates in a biological system. In general, it was found that ω B97XD/6-311G(2d,p) gave the most reasonable structures and thermochemistry relative to benchmark calculations. However, nuances in performance are observed and discussed.

Keywords: DFT; cysteine polysulfide; reactive sulfur species; gas phase basicity; proton affinity; bond dissociation enthalpy; hydrogen affinity; thermochemistry

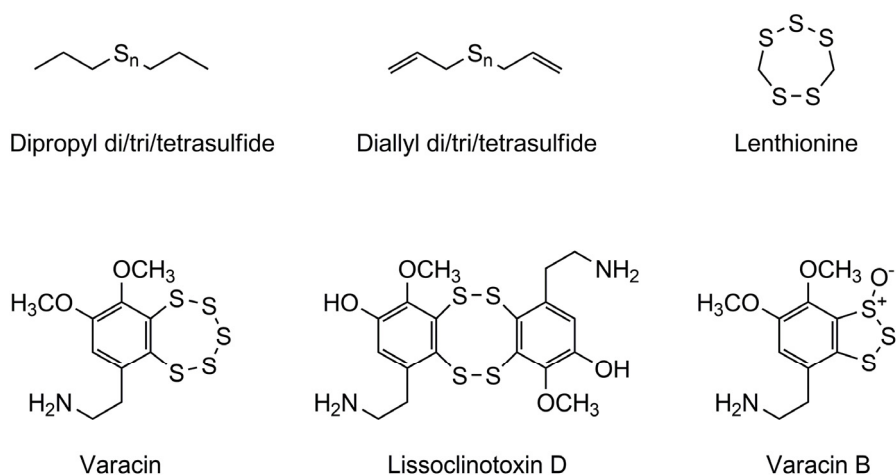
1. Introduction

The chalcogens sulfur and selenium have long been known to play key roles in a diverse array of important physiological and biological processes including enzymatic mechanisms [1,2], signaling [3–5], and mediation and repair of oxidatively damaged biomolecules [6–8]. Indeed, in addition to being found within three of the 22 proteinogenic amino acids—cysteine (Cys), methionine (Met), and selenocysteine (Sec)—they are also found in many essential metabolites (e.g., thiazole). This is due to their ability to possess a broad range of oxidation states as well as bonding environments, and they can often undergo reversible redox [9]. For instance, the most abundant antioxidant in animal

cells is glutathione (GSH), which can mediate the cellular redox environment through interconversion with its oxidized disulfide form, GSSG [10].

Recently, it has increasingly been recognized that reactive sulfur species (RSS) comprise a rich and diverse range of physiologically important species (Scheme 1) [11]. Indeed, hydrogen sulfide is now known to be a ubiquitous essential signaling molecule that plays key roles in many physiological and inflammatory processes including blood pressure regulation, cell proliferation and apoptosis, insulin signaling, and neurotransmission [7,12–16]. However, sulfur can also form strong homonuclear single bonds and, as a result, can react with other sulfur species (for example, in proteins) to form a variety of polysulfur-containing RSS [17].

Previously, the presence of per- (HSSH) and polysulfides (e.g., H_2S_n , $n = 3-7$) in biological systems was thought to be an experimental artifact or store for H_2S [18]. Now, however, they are increasingly proposed or recognized as being biochemically important [17,19–22]; for instance, some polysulfides have been shown to possess antibiotic or anticancer properties [23,24]. More recently, CysteinyI-tRNA synthetase (CysRS), an ancient enzyme with a critical role in gene-encoded protein synthesis, has also been shown to catalyze the formation of Cys-derived polysulfides [21]. This further underscores the potential biologically important activity of peptide-derived hydropersulfides [25]. Meanwhile, Se has been shown to form an Se–S intermediate in the selenoproteins thioredoxin reductase and formate dehydrogenase and plays a central role in the enzyme's activation [26,27]. Unfortunately, due to the high reactivity of RSS, specifically per-/polysulfides within biological environments, many of their properties and much of their chemistry remain unclear or even unknown.

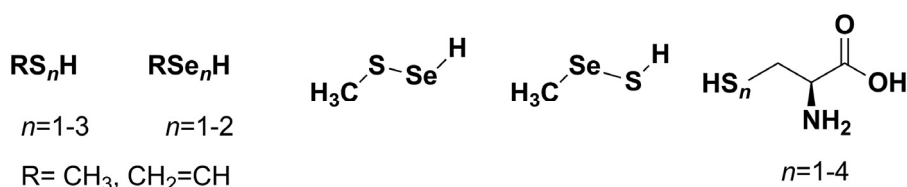


Scheme 1. Several examples of naturally occurring polysulfur species [17,28].

Computational chemistry has established itself as a key tool for the study of the properties and chemistry of biomolecular systems. Several such studies have been performed on S- and, to a notably lesser extent, Se- or mixed S/Se-containing per- and poly-seleno/sulfides. For example, Brzostowska et al. used the B3LYP method to examine the intramolecular reactions of the naturally occurring polysulfur-containing pentathiepins (such as varacin, Scheme 1) that generate S_3 and S_2 transfer units via a tetra- or trisulfide anion, respectively [29]. Recently, the high reactivity of several smaller hydropersulfides toward alkyl, alkoxy, peroxy, and thyl radicals was investigated using both experimental and computational (CBS-QB3) methods [30]. It was concluded that such reactions are exothermic by 15–34 kcal mol⁻¹ due to the low RSS–H bond dissociation enthalpy and high stability of perthiyl radicals [30]. Meanwhile, a computational study has used dispersion-corrected B3LYP (B3LYP-D3) to examine the role of the chalcogen atoms in the mechanism of glutathione peroxidase 4, which involves formation of a –Se–S– species [31]. Bachrach et al. used several computational methods including MP2 and B3LYP to examine possible mechanisms for nucleophilic attack at the Se in diselenides and selenosulfides and concluded that attack at Se is kinetically and thermodynamically

preferred [32]. Using an ONIOM QM/MM approach, wherein the DFT method M06-2X was used for the QM region, Huang et al. examined S-sulfhydration via a persulfide (RSS^-) intermediate as catalyzed by mercaptopyruvate sulfurtransferase (MST) and obtained reasonable agreement with the experiment [33]. In all of these studies, smaller basis sets (e.g., 6-31G(d)) were used to obtain structures upon which they then based their calculations of thermochemical properties. The ability of a computational study to reliably and accurately provide insights into the structures and properties of any biomolecular system usually critically depends on the choice of QM method and basis set. Thus, an essential step towards computationally studying RSS is determining appropriate methodologies.

In this present study, the ability of a range of computational, in particular density functional theory (DFT) methods [34] to provide reliable and accurate structures and thermochemical properties of biologically relevant poly-sulfur/selenium containing compounds has been assessed. More specifically, the DFT methods B3LYP, B3PW91, ω B97XD, M06-2X, and M08-HX were applied to a systematic series of biologically relevant $\text{RX}_n(\text{H})$ ($X = \text{S}/\text{Se}$, $n = 1-3$, $\text{R} = \text{CH}_3$, $\text{CH}_2=\text{CH}$ and cysteine, Scheme 2) species. As well as their structures, a variety of key thermochemical properties including their X–X (chalcogen–chalcogen) bond dissociation enthalpies, hydrogen affinities, and gas phase basicities were examined and benchmarked.



Scheme 2. Schematic illustration of the species considered in this study.

2. Results and Discussion

Structural Assessment of CH_3XXH and CH_3XX^- ($X = \text{S}, \text{Se}$). We began by using the broadest variety of DFT methods (B3LYP, B3PW91, ω B97XD, M06-2X, M08-HX) and range of basis sets (6-31G(d) to 6-311++G(3df,3pd)) used in this study to obtain optimized structures for CH_3XXH and CH_3XX^- ($X = \text{S}, \text{Se}$). These are the smallest homoatomic persulf/selenides considered in this present study. Due to a paucity of corresponding experimental data, benchmark optimized structures were obtained at the QCISD/6-311+G(2df,p) level of theory. For simplicity, only the key C–X, X–X, and X–H ($X = \text{S}, \text{Se}$) distances are discussed herein and summarized in Table 1; MP2 data are shown in Table S1.

Table 1. Selected optimized bond lengths (in ångströms; Å) for CH_3XXH and CH_3XX^- ($X = \text{S}, \text{Se}$).

Method	Basis Set	CH_3SSH			CH_3SS^-		CH_3SeSeH			CH_3SeSe^-	
		C–S	S–S	S–H	C–S	S–S	C–Se	Se–Se	Se–H	C–Se	Se–Se
B3LYP	6-31G(d)	1.834	2.091	1.357	1.837	2.117	1.977	2.337	1.495	1.985	2.366
	6-311G(d)	1.830	2.103	1.357	1.831	2.134	1.979	2.362	1.488	1.987	2.391
	6-311G(d,p)	1.831	2.105	1.354	1.833	2.134	1.978	2.364	1.478	1.987	2.391
	6-311+G(d,p)	1.830	2.103	1.354	1.832	2.128	1.978	2.364	1.478	1.987	2.388
	6-311G(2d,p)	1.830	2.088	1.349	1.831	2.115	1.975	2.366	1.476	1.984	2.395
	6-311G(df,p)	1.829	2.093	1.354	1.831	2.120	1.973	2.351	1.479	1.981	2.376
	6-311+G(2df,p)	1.825	2.072	1.351	1.827	2.092	1.971	2.350	1.477	1.979	2.373
	6-311++G(3df,3pd)	1.820	2.064	1.349	1.822	2.083	1.971	2.351	1.476	1.978	2.373
B3PW91	6-31G(d)	1.821	2.072	1.354	1.824	2.096	1.961	2.315	1.491	1.960	2.336
	6-311G(d)	1.817	2.081	1.356	1.819	2.110	1.963	2.338	1.486	1.963	2.361
	6-311G(d,p)	1.818	2.083	1.353	1.820	2.110	1.962	2.340	1.476	1.962	2.360
	6-311+G(d,p)	1.818	2.083	1.353	1.821	2.105	1.962	2.339	1.476	1.962	2.358
	6-311G(2d,p)	1.817	2.067	1.349	1.819	2.091	1.959	2.342	1.474	1.959	2.363
	6-311G(df,p)	1.816	2.072	1.353	1.818	2.097	1.957	2.327	1.477	1.958	2.345
	6-311+G(2df,p)	1.812	2.053	1.351	1.814	2.071	1.955	2.327	1.475	1.955	2.342
	6-311++G(3df,3pd)	1.808	2.046	1.349	1.810	2.063	1.955	2.327	1.475	1.955	2.342

Table 1. Cont.

Method	Basis Set	CH ₃ SSH			CH ₃ SS [−]		CH ₃ SeSeH			CH ₃ SeSe [−]	
		C–S	S–S	S–H	C–S	S–S	C–Se	Se–Se	Se–H	C–Se	Se–Se
ωB97XD	6-31G(d)	1.819	2.070	1.349	1.821	2.095	1.954	2.309	1.486	1.968	2.342
	6-311G(d)	1.816	2.079	1.350	1.816	2.110	1.957	2.331	1.480	1.971	2.365
	6-311G(d,p)	1.816	2.081	1.348	1.817	2.110	1.956	2.333	1.470	1.970	2.365
	6-311+G(d,p)	1.816	2.080	1.348	1.817	2.105	1.956	2.333	1.470	1.970	2.362
	6-311G(2d,p)	1.816	2.067	1.344	1.816	2.092	1.953	2.334	1.469	1.967	2.369
	6-311G(df,p)	1.815	2.070	1.348	1.815	2.099	1.951	2.320	1.472	1.965	2.351
	6-311+G(2df,p)	1.810	2.053	1.346	1.811	2.074	1.950	2.319	1.470	1.963	2.348
6-311++G(3df,3pd)	1.806	2.046	1.344	1.807	2.066	1.949	2.320	1.469	1.962	2.347	
M06-2X	6-31G(d)	1.819	2.069	1.348	1.819	2.096	1.954	2.306	1.486	1.985	2.366
	6-311G(d)	1.816	2.078	1.348	1.816	2.110	1.960	2.330	1.480	1.964	2.358
	6-311G(d,p)	1.817	2.079	1.346	1.817	2.110	1.959	2.331	1.472	1.964	2.358
	6-311+G(d,p)	1.816	2.089	1.346	1.816	2.105	1.959	2.331	1.472	1.964	2.355
	6-311G(2d,p)	1.817	2.066	1.342	1.816	2.093	1.956	2.334	1.471	1.961	2.362
	6-311G(df,p)	1.814	2.068	1.347	1.816	2.097	1.954	2.320	1.473	1.960	2.345
	6-311+G(2df,p)	1.811	2.052	1.345	1.812	2.073	1.953	2.319	1.472	1.958	2.340
6-311++G(3df,3pd)	1.808	2.046	1.342	1.808	2.065	1.953	2.319	1.472	1.958	2.341	
M08-HX	6-31G(d)	1.817	2.068	1.350	1.817	2.094	1.955	2.305	1.488	1.958	2.330
	6-311G(d)	1.816	2.078	1.345	1.815	2.108	1.961	2.327	1.482	1.964	2.352
	6-311G(d,p)	1.816	2.079	1.348	1.815	2.108	1.960	2.328	1.474	1.963	2.352
	6-311+G(d,p)	1.816	2.079	1.349	1.815	2.103	1.960	2.328	1.474	1.964	2.348
	6-311G(2d,p)	1.814	2.067	1.344	1.814	2.093	1.957	2.331	1.473	1.960	2.357
	6-311G(df,p)	1.814	2.069	1.349	1.814	2.095	1.954	2.318	1.475	1.959	2.341
	6-311+G(2df,p)	1.809	2.053	1.347	1.810	2.072	1.953	2.317	1.474	1.957	2.335
6-311++G(3df,3pd)	1.807	2.047	1.344	1.808	2.063	1.953	2.318	1.472	1.957	2.336	
QCISD	6-311+G(2df,p)	1.815	2.065	1.347	1.816	2.088	1.965	2.333	1.474	1.961	2.359

Method Sensitivity to Basis Set Changes: All five DFT methods showed similar overall sensitivities to changes in the basis set from 6-31G(d) to 6-311++G(3df,3pd). For example, the smallest variations were observed for the C–X and X–H (X = S, Se) bond distances; for any given method and chemical system (be it neutral or anionic) they varied by ≤ 0.020 Å. The only exceptions occurred for the C–Se bond in CH₃SeSe[−] when using M06-2X method, which varied overall by 0.027 Å, and the Se–H bond using MP2, which varied by 0.025 Å (Table S1). Notably, for any DFT method and chemical system the C–S bond distances showed greater variation than that of C–Se bonds. The only exceptions to this trend occurred for the C–X bonds in the CH₃XX[−] anions when using the B3LYP or M06-2X methods. However, the reverse trend was observed for the X–H bonds; optimized Se–H bond lengths are more sensitive to basis set choice than S–H bonds (Table 1 and Table S1).

For all chemical systems (both neutral and anionic), regardless of the choice of DFT method, the largest variations upon changing basis set were observed in their X–X bonds. For CH₃SSH and CH₃SS[−] it was found that the S–S bond distances varied by 0.032–0.043 and 0.044–0.051 Å, respectively. Meanwhile, in the corresponding CH₃SeSeH and CH₃SeSe[−] species the Se–Se bond distances varied by 0.024–0.029 and 0.023–0.029 Å, respectively, except for using MP2 where the variation exceeded the trend for DFT data (Table S1). That is, except for Se–H bonds, those bonds involving sulfur (i.e., C–X and X–X) in CH₃XXH and CH₃XX[−] (X = S, Se) are most sensitive to the choice of basis set.

Effects of Increasing Basis Set Size: As can be seen in Table 1, for all DFT methods considered and for both neutral CH₃XXH and anionic CH₃XX[−] (X = S, Se), similar trends were generally observed upon increasing the basis set from double- to triple-zeta, and then subsequently by inclusion of diffuse and polarization functions.

For instance, increasing the basis set from 6-31G(d) to 6-311++G(3df,3pd) generally caused a systematic shortening in the X–H and C–X bonds. Notably, one does not need to increase the basis set significantly in order to get reasonable agreement with the corresponding values obtained at the QCISD/6-311+G(2df,p) level of theory. In fact, upon changing the basis set from 6-31G(d) to 6-311G(d) (i.e., double- to triple-zeta) resulted in their lengths differing from the benchmark values by ≤ 0.015 Å. Further increases in basis set size by inclusion of diffuse (i.e., 6-311G(d,p) to 6-311+G(d,p)) or *f*- and/or *d*-polarization functions on heavy atoms or hydrogen resulted in only minor individual decreases.

In contrast, modifying the basis set showed quite different trends for the X–X (X = S, Se) bonds. For instance, for all methods assessed, improving the basis set from 6-31G(d) to 6-311G(d) resulted in an increase in their optimized length for all chemical systems of up to 0.025 Å. The only exception occurred for the M06-2X method applied to CH₃SeSe[−] for which the Se–Se bond shortened slightly by 0.008 Å. Notably, in CH₃SSH and CH₃SS[−] the observed ranges of bond lengthening were 0.009–0.015 and 0.014–0.027 Å, respectively, with the largest increases observed when using the B3LYP method. That is to say, the anionic persulfide is more sensitive to basis set changes than the neutral hydropersulfide. In contrast, for CH₃SeSeH and CH₃SeSe[−] the observed increases were quite similar lying in the range of 0.017–0.025 Å (except where noted above). The further inclusion of *p*-functions on hydrogen (i.e., 6-311G(d) to 6-311G(d,p)) or diffuse functions on heavy atoms (i.e., 6-311G(d,p) to 6-311+G(d,p)) had negligible effect on the X–X bond lengths in both the neutral CH₃XXH and anionic CH₃XX[−] (X = S, Se) systems.

In general, more significant changes in the X–X lengths were observed upon inclusion of either a second set of *d*- or a set of *f*-functions on heavy atoms (i.e., 6-311G(d,p) to 6-311G(2d,p) or 6-311G(df,p)). Specifically, for both these basis set changes the S–S bonds in CH₃SSH and CH₃SS[−] shortened by 0.010 to 0.017 Å, except for MP2 where the distance increases for the 6-311G(2d,p) basis set. In contrast, for the corresponding selenium containing systems, the inclusion of a second set of *d*-functions on heavy atoms marginally lengthened Se–Se bonds by ≤ 0.004 Å, while the inclusion of a set of *f*-functions on heavy atoms shortened the Se–Se bonds by 0.010–0.017 Å. Combining or adding further diffuse and polarization functions by use of the 6-311+G(2df,p) or 6-311++G(3df,3pd) basis sets respectively, resulted in all DFT methods except B3LYP giving X–X (X = S, Se) bond lengths that were markedly shorter than their corresponding benchmark values. In the case of B3LYP (which overestimates the length of these bonds) increasing the basis set to 6-311+G(2df,p) or 6-311++G(3df,3pd) was in fact required in order to get good agreement with the benchmark values.

Importantly, for all DFT methods that were considered (with the exception of B3LYP), the 6-311G(2d,p) and 6-311G(df,p) basis sets gave optimized C–X, X–X, and X–H distances for CH₃XXH and CH₃XX[−] (X = S) that were in closest general agreement with their corresponding benchmark values. Meanwhile, for the corresponding Se analogues, the best performing basis sets were generally 6-311G(d), 6-311G(d,p), 6-311+G(d,p), and 6-311G(2d,p). It is also noted that the M08-HX method does not offer much if any improvement over M06-2X. In fact, when Se is in the system, it slightly underestimates the bond lengths. As such, subsequent tables showing optimized parameters will only include results obtained using the B3PW91, ωB97XD and M06-2X methods in combination with the identified preferred basis sets. It should be noted that, for completeness, the corresponding values for the other methods are included in the Supplementary Materials. Since MP2 trends were mostly similar to DFT, we do not include results obtained with this method.

Effect of Conjugation: CH₂CHXXH and CH₂CHXX[−] (X = S, Se). These model systems were examined to gain insights into the influence of conjugation on the neutral and anionic persulfide and perselenide groups. Based on the results obtained for the CH₃XX[−]/H systems, optimized structures were obtained using only the B3PW91, ωB97XD, and M06-2X methods in combination with the 6-311+G(d,p), 6-311G(2d,p), and 6-311G(df,p) basis sets. The most significant changes were observed in their C–X and X–X bonds, hence only these optimized values are shown in Table 2. Table S2 includes the full set of optimized parameters with all DFT functionals and the X–H bonds.

Table 2. Selected optimized bond lengths (in ångstroms; Å) for CH₂CHXXH and CH₂CHXX[−] (X = S, Se).

Method	Basis Set	CH ₂ CHSSH		CH ₂ CHSS [−]		CH ₂ CHSeSeH		CH ₂ CHSeSe [−]	
		C–S	S–S	C–S	S–S	C–Se	Se–Se	C–Se	Se–Se
B3PW91	6-311+G(d,p)	1.768	2.088	1.745	2.098	1.913	2.347	1.899	2.359
	6-311G(2d,p)	1.767	2.074	1.747	2.084	1.910	2.350	1.898	2.364
	6-311G(df,p)	1.768	2.077	1.748	2.090	1.908	2.334	1.894	2.346
ωB97XD	6-311+G(d,p)	1.771	2.084	1.748	2.101	1.913	2.338	1.898	2.357
	6-311G(2d,p)	1.770	2.072	1.750 ^a	2.088 ^a	1.910	2.339	1.897	2.361
	6-311G(df,p)	1.770	2.074	1.751	2.096	1.908	2.325	1.895	2.343
M06-2X	6-311+G(d,p)	1.770	2.084	1.747	2.102	1.914	2.337	1.901	2.354
	6-311G(2d,p)	1.770	2.071	1.751	2.090	1.911	2.340	1.900	2.359
	6-311G(df,p)	1.770	2.072	1.750	2.095	1.909	2.326	1.897	2.343
QCISD	6-311+G(2df,p)	1.771	2.069	1.750	2.086	1.914	2.329	1.902	2.359

^a Had one negligible imaginary frequency.

In general, upon changing basis sets and methods similar trends were observed as for the CH₃XX[−]/H systems, though with some key differences. For instance, for X = S, the closest agreement of the optimized bond lengths with the benchmark values was obtained for the 6-311G(df,p) and 6-311G(2d,p) basis sets. In contrast, for X = Se the X–X bond is more sensitive to the choice of basis set. In particular, for CH₂CHSeSe[−] the best agreement with the benchmark values are obtained using the 6-311+G(d,p) or 6-311G(2d,p) basis sets; inclusion of *f*-functions results in too short an Se–Se bond. Meanwhile, for neutral CH₂CHSeSeH it is essential to include *f*-functions in order to obtain good agreement with the corresponding benchmark values.

Comparison of the optimized bond lengths in CH₃XX[−]/H and CH₂CHXX[−]/H (X = S, Se) shows that for all species, at all levels of theory, the optimized C–X distance in CH₂CHXX[−]/H is 0.04–0.05 Å shorter than in the corresponding CH₃XX[−]/H analogue (cf. Table 1). This is also observed when structures are optimized at the M06-2X/aug-cc-pVTZ level of theory (data not shown). In contrast, the X–X bond lengths in CH₂CHXX[−]/H (X = S, Se) are all within ±0.01 Å of their optimized values in the corresponding CH₃XX[−]/H analogue. When X = S the X–X bond in the anion is 0.017 Å longer in the conjugated species compared to 0.023 Å in the alkyl terminated species. It is noted that this again indicates that deprotonation of RXXH (X = S, Se) causes the X–X bond to lengthen, although conjugation lessens the bond lengthening upon going to the anion.

Effects of Mixed Sulfur/Selenium: CH₃XYH (X = S, Se; Y = Se, S). We then considered mixed sulfur/selenide species for which selected optimized parameters are given in Table 3. Full optimized parameters for all DFT methods and basis sets are shown in Table S3.

Table 3. Selected optimized bond lengths (in ångstroms; Å) for CH₃XYH and CH₃XY[−] (X = S, Se; Y = Se, S).

Method	Basis Set	CH ₃ SSeH		CH ₃ SSe [−]		CH ₃ SeSH		CH ₃ SeS [−]	
		C–S	S–Se	C–S	S–Se	C–Se	Se–S	C–Se	Se–S
B3PW91	6-311+G(d,p)	1.821	2.214	1.820	2.256	1.959	2.218	1.971	2.221
	6-311G(2d,p)	1.819	2.204	1.819	2.244	1.957	2.208	1.968	2.220
	6-311G(df,p)	1.819	2.199	1.819	2.241	1.953	2.204	1.964	2.212
ωB97XD	6-311+G(d,p)	1.820	2.208	1.817	2.252	1.953	2.213	1.962	2.218
	6-311G(2d,p)	1.818	2.199	1.817	2.242	1.951	2.204	1.959	2.216
	6-311G(df,p)	1.818	2.195	1.817	2.239	1.948	2.200	1.957	2.209
M06-2X	6-311+G(d,p)	1.819	2.208	1.817	2.250	1.956	2.212	1.964	2.220
	6-311G(2d,p)	1.817	2.200	1.816	2.239	1.954	2.203	1.960	2.221
	6-311G(df,p)	1.817	2.194	1.816	2.237	1.951	2.198	1.959	2.212
QCISD	6-311+G(2df,p)	1.819	2.198	1.816	2.239	1.952	2.202	1.961	2.207

For all four mixed species the optimized lengths of the C–X bond (X = S, Se) are all within 0.01 Å of those obtained for their analogous persulfide or perselenide (i.e., CH₃XXH (X = S, Se)) at the same level of theory (cf. Table 1). Thus, a similar method and basis set trends were also observed and

do not require further detailed discussion. However, it should be noted that, while the X–Y bond lengths in the neutral species CH_3SSeH and CH_3SeSH are close to each other, the bond is consistently predicted to be marginally shorter ($<0.01 \text{ \AA}$) in CH_3SSeH . The changes observed in the $\text{CH}_3\text{X–Y}$ bond length upon deprotonation (*i.e.*, CH_3XYH to CH_3XY^-), depends on whether S or Se is the terminal atom. When S is the terminal atom, upon deprotonation of the thiol group the Se–S bond lengthens marginally by $<0.01 \text{ \AA}$. In contrast, when Se is the terminal atom deprotonation causes the S–Se bond to lengthen by $\geq 0.04 \text{ \AA}$. The larger impact of deprotonating a selenol versus thiol group is also seen in the species shown in Tables 1 and 2, though to a smaller extent. We found that when the sulfur atom is in the middle of the chain, it has a larger Mulliken charge compared to selenium (-0.23 vs. -0.13) in the anionic species. By comparison, the charge of the terminal chalcogen is the same in both species. Thus, repulsive interactions cause the bond length to increase when sulfur is in the center of the chain.

Extending a Sulfide: CH_3SSSH and CH_2CHSSH . Polysulfides, but to-date not polyselenides, have been suggested to be potentially biochemically important. Thus, for completeness, we considered the effect of extending the persulfide chain. Specifically, the simplest alkyl- and conjugate-containing trisulfides, CH_3SSSH and CH_2CHSSH , were examined. The C– S_1 bond in all species had very similar optimized lengths (see Table S4 in the Supplementary Materials), for all methods and basis sets used, to those obtained for the analogous alkyl persulfides (cf. Table 1); the observed shortened C–X bond in the conjugated neutral and anionic persulfides (Table 2) was not observed in CH_2CHSSH , further evidence that it is due to delocalization across the persulf/selenide and conjugated R-group (see Supplementary Materials). Thus, in Table 4 only the optimized lengths of the S–S bonds are given.

As can be seen in Table 4, the B3PW91 method gives the worst agreement with the benchmark values, especially for the deprotonated (anionic) species with errors of up to 0.07 \AA . Furthermore, for any DFT method, the largest errors in the optimized $\text{S}_i\text{–S}_j$ bond lengths are observed upon use of the 6-311+G(d,p) basis set. The best agreement is instead obtained using the M06-2X and ωB97XD methods, the former performing slightly better in conjunction with the 6-311G(2d,p) basis set. Indeed, their errors lie in the ranges of $0.000\text{–}0.011 \text{ \AA}$ and $-0.003\text{–}0.009 \text{ \AA}$, respectively.

Table 4. Selected optimized bond lengths (in ångstroms; Å) for RSSSH ($\text{R} = \text{CH}_3, \text{CH}_2\text{CH}$).

Method	Basis Set	CH_3SSSH		CH_3SSS^-		CH_2CHSSH		CH_2CHSS^-	
		$\text{S}_1\text{–S}_2$	$\text{S}_2\text{–S}_3$	$\text{S}_1\text{–S}_2$	$\text{S}_2\text{–S}_3$	$\text{S}_1\text{–S}_2$	$\text{S}_2\text{–S}_3$	$\text{S}_1\text{–S}_2$	$\text{S}_2\text{–S}_3$
B3PW91	6-311+G(d,p)	2.069	2.102	2.147	2.067	2.082	2.094	2.170	2.052
	6-311G(2d,p)	2.057	2.086	2.120	2.058	2.071	2.079	2.136	2.047
	6-311G(df,p)	2.060	2.091	2.130	2.063	2.073	2.084	2.149	2.050
ωB97XD	6-311+G(d,p)	2.068	2.093	2.124	2.073	2.078	2.086	2.134	2.062
	6-311G(2d,p)	2.057	2.080	2.105	2.063	2.070	2.074	2.115	2.054
	6-311G(df,p)	2.059	2.084	2.111	2.070	2.071	2.077	2.123	2.060
M06-2X	6-311+G(d,p)	2.066	2.090	2.121	2.074	2.079	2.083	2.143	2.063
	6-311G(2d,p)	2.056	2.078	2.103	2.065	2.070	2.071	2.118	2.055
	6-311G(df,p)	2.057	2.080	2.107	2.069	2.070	2.073	2.123	2.060
QCISD	6-311+G(2df,p)	2.056	2.078	2.096	2.065	2.066	2.073	2.107	2.057

Notably, in CH_3SSSH and CH_2CHSSH , the $\text{CS}_1\text{–S}_2$ bond is predicted to be shorter than the $\text{S}_2\text{–S}_3\text{H}$ bond by >0.02 and $<0.01 \text{ \AA}$, respectively. However, upon deprotonation of the terminal thiol group in each, *i.e.*, formation of CH_3SSS^- and CH_2CHSS^- , the $\text{CS}_1\text{–S}_2$ bond lengthens significantly by $\sim 0.05 \text{ \AA}$, from ~ 2.06 and 2.07 \AA in CH_3SSSH and CH_2CHSSH , respectively, to approximately 2.1 and 2.12 \AA . In contrast, the $\text{S}_2\text{–S}_3$ bond in CH_3SSS^- and CH_2CHSS^- has shortened by $0.01\text{–}0.02 \text{ \AA}$. Mulliken charges on S_1 were found to decrease more than they do on S_2 upon deprotonation in the benchmark calculation, for both alkyl and conjugated polysulfur species. However, the difference between the two was small compared to the large charge on S_3 ; it becomes much more negative upon deprotonation. This indicates that there is some degree of charge delocalization along the sulfur chain (Table S5).

Obtaining Reliable and Accurate Thermochemistry for CH₃SSH and CH₂CHSSH. Two of the most common goals when applying computational methods to the study of chemical problems are obtaining reliable and accurate optimized structures and thermochemical data. For biochemical or related problems, common reactions often require knowledge of proton affinities (PAs), gas phase basicities (GPBs), hydrogen affinities (HAs) and bond dissociation enthalpies (BDEs). Furthermore, given the size of the systems often encountered there is simultaneously considerable interest in identifying a DFT-based approach for calculating such properties. Thus, having assessed the use of DFT methods for the accurate optimization of structures, we also assessed the ability of the DFT methods B3LYP, B3PW91, ω B97XD, M06-2X, M08-HX, in combination with a range of basis sets to provide reliable and accurate biochemically-relevant thermochemical data.

Given the poor performance of B3LYP and minimal improvement of M08-HX over M06-2X in obtaining reliable structures, *vide supra*, here we only report the performance of B3PW91, ω B97XD, and M06-2X, unless otherwise noted. Furthermore, we have focused on reporting basis sets that for such systems have been previously used (e.g., 6-31G(d)), shown herein to be most consistently reliable (i.e., 6-311G(2d,p)), or often used for calculating accurate thermochemistry (i.e., 6-311+G(2df,p) and 6-311++G(3df,3pd)). The results obtained are summarized in Table 5, although the data for all functionals and basis sets that were studied are shown in Tables S6–S11.

Table 5. Homolytic S–S bond dissociation enthalpy (BDE) of RSSH, proton affinity (PA) and gas-phase basicity (GPB) of RSS[−], and hydrogen affinity (HA) of RSS[•] (R = CH₃, CH₂CH). All energies calculated at 298.15K and in kJ mol^{−1} (see Section 3).

Method	Basis Set	CH ₃ SSH	CH ₃ SS [−]		CH ₃ SS [•]
		BDE(S–S)	PA	GPB	HA
B3PW91	6-31G(d)	235.4	1455.2	1424.8	274.6
	6-311G(2d,p)	250.3	1447.7	1417.3	283.8
	6-311+G(2df,p)	254.7	1445.8	1415.4	279.5
	6-311++G(3df,3pd)	255.8	1448.7	1418.4	281.6
ω B97XD	6-31G(d)	244.1	1455.0	1425.1	284.0
	6-311G(2d,p)	258.5	1447.3	1417.5	292.0
	6-311+G(2df,p)	264.6	1445.5	1415.8	288.0
	6-311++G(3df,3pd)	265.6	1449.2	1419.6	289.8
M06-2X	6-31G(d)	252.0	1440.0	1411.4	285.4
	6-311G(2d,p)	264.9	1430.0	1401.6	294.4
	6-311+G(2df,p)	270.3	1428.5	1400.1	291.0
	6-311++G(3df,3pd)	272.3	1432.3	1404.2	293.9
QCISD	6-311+G(2df,p)	236.3	1445.4	1415.1	282.7
Method	Basis Set	CH ₂ CHSSH	CH ₂ CHSS [−]		CH ₂ CHSS [•]
		BDE(S–S)	PA	GPB	HA
B3PW91	6-31G(d)	238.0	1427.6	1396.5	272.8
	6-311G(2d,p)	253.0	1423.1	1391.5	282.1
	6-311+G(2df,p)	255.7	1417.7	1386.8	278.4
	6-311++G(3df,3pd)	256.8	1420.5	1389.7	280.1
ω B97XD	6-31G(d)	244.1	1429.8	1397.3	283.7
	6-311G(2d,p)	258.5	1422.4 ^a	1395.9 ^a	291.5
	6-311+G(2df,p)	262.7	1420.2	1382.0	288.3
	6-311++G(3df,3pd)	263.5	1423.6	1388.7	289.7
M06-2X	6-31G(d)	249.8	1414.5	1381.1	283.7
	6-311G(2d,p)	263.0	1408.2	1374.4	292.8
	6-311+G(2df,p)	267.4	1403.4	1366.4	290.2
	6-311++G(3df,3pd)	269.1	1406.7	1368.1	292.6
QCISD	6-311+G(2df,p)	242.0	1421.8	1390.7	283.5

^a One of the required species for determining this value had one negligible imaginary frequency.

The benchmark values were again obtained using the QCISD/6-311+G(2df,p) level of theory. The thermochemical values obtained for the conjugated persulfides compared to the alkyl persulfides reflects the trends observed structurally. For instance, the BDE(S–S) for CH₂CHSSH is slightly higher by 5.7 kJ mol^{−1} than that of CH₃SSH, while the PA and GPB of CH₂CHSS[−] are 23.6 and 24.4 kJ mol^{−1} lower, respectively, than those of CH₃SS[−]. This is due to delocalization across the persulfide and CH₂CH group in CH₂CHSSH/[−]. Meanwhile, the hydrogen affinity of CH₂CHSS• is predicted to be only marginally higher than that of CH₃SS• by 0.8 kJ mol^{−1}. Notably, we did see spin contamination in the QCISD calculations with a spin of 0.88. This may be the reason for lower energies calculated by QCISD compared to DFT methods where spin contamination was much lower (0.77).

A DFT-based model was determined to be accurate if it gave values within 10 kJ mol^{−1}, generally held to be experimental accuracy, of the benchmark values. From Table 5 it can be seen that not all methods or basis set choices were reliable, nor did all thermochemical properties exhibit the same method/basis set requirement. For instance, for accurate determination of the BDE(S–S) of both CH₃SSH and CH₂CHSSH, the best performance was observed for B3PW91 and ωB97XD in combination with the 6-31G(d) basis set. The former method slightly underestimating compared to the benchmark value while the latter overestimated slightly. The M06-2X method only gave an accurate BDE(S–S) for CH₂CHSSH and again when using the 6-31G(d) basis set. In general, the use of basis sets larger than 6-31G(d) gave BDE(S–S) values that are markedly higher (14–36 kJ mol^{−1}) than those obtained at the QCISD/6-311+G(2df,p) level of theory.

For the PA and GPB of the CH₃SS[−] and CH₂CHSS[−] anions the M06-2X method again only gives accurate values when used in combination with the 6-31G(d) basis set. In contrast, the B3PW91 and ωB97XD give accurate values for all the basis sets considered. However, the triple-zeta basis sets (6-311G(2d,p), 6-311+G(2df,p), and 6-311++G(3df,3pd)) gave best agreement with calculated values within 5 kJ mol^{−1} of their corresponding benchmark value (see Table 5).

The calculated values of the hydrogen affinity of CH₃SS• and CH₂CHSS• follow almost the same method and basis set trends and accuracy as that observed for the PA and GPB of CH₃SS[−] and CH₂CHSS[−]. Namely, the B3PW91 and ωB97XD methods in conjunction with any of the basis sets considered give calculated values within ±10 kJ mol^{−1}. The only exception occurs when at the B3PW91/6-31G(d) level of theory for CH₂CHSS•, which gives a HA value 10.7 kJ mol^{−1} lower than the corresponding QCISD/6-311+G(2df,p) benchmark value (see Table 5). Meanwhile, the M06-2X method is inconsistent; for CH₃SS• only the 6-31G(d) and 6-311+G(2df,p) basis sets give values within 10 kJ mol^{−1} of the benchmark values while for CH₂CHSS• it gives good agreement for all basis sets considered herein.

Several overall trends are suggested in this examination of the performance of the DFT methods B3PW91, ωB97XD, and M06-2X, in conjunction with a range of basis sets, for the noted important thermochemical properties. In particular, the M06-2X functional is the least consistent and usually gives values that differ from the benchmark values by more than 10 kJ mol^{−1}. Furthermore, for all DFT functionals the values obtained using the 6-311+G(2df,p) basis set are within 4 kJ mol^{−1} of the corresponding values obtained using the much larger and more expensive 6-311++G(3df,3pd) basis set. Hence, for the remainder of this report, for simplicity, only thermochemical values obtained using the B3PW91 and ωB97XD functionals in combination with basis sets no larger than 6-311+G(2df,p) are discussed, unless otherwise noted (see Tables S6–S11 for the complete datasets).

Thermochemistry of Selenium-Containing Species. As noted above in the structural assessment, for selenium containing species considered herein; that is CH₃SeSe•/[−]/H, CH₂CHSeSe•/[−]/H, CH₃SSe•/[−]/H, and CH₃SeS•/[−]/H, the smallest consistently reliable basis set was 6-311+G(d,p), though with exceptions as noted. Hence, for these species we have limited our discussion herein to results obtained using B3PW91 and ωB97XD in conjunction with the 6-311+G(d,p) and 6-311+G(2df,p) basis sets. The results are shown in Table 6.

Table 6. Calculated homolytic Se–Se bond dissociation enthalpies (BDE) of RSeSeH, proton affinity (PA) and gas-phase basicities (GPB) of RSeSe[−], and Se–H homolytic bond dissociation enthalpies (HA) of RSeSe• (R = CH₃, CH₂CH). All energies in kJ mol^{−1}.

Method	Basis Set	CH ₃ SeSeH	CH ₃ SeSe [−]		CH ₃ SeSe•
		BDE(Se–Se)	PA	GPB	HA
B3PW91	6-311+G(d,p)	219.2	1409.0	1378.7	270.5
	6-311+G(2df,p)	222.9	1411.4	1381.1	266.0
ωB97XD	6-311+G(d,p)	218.0	1410.8	1380.7	276.5
	6-311+G(2df,p)	222.6	1413.3	1383.4	270.7
QCISD	6-311+G(2df,p)	204.1	1404.3	1374.0	267.3
Method	Basis Set	CH ₂ CHSeSeH	CH ₂ CHSeSe [−]		CH ₂ CHSeSe•
		BDE(Se–Se)	PA	GPB	HA
B3PW91	6-311+G(d,p)	222.1	1388.6	1357.4	270.2
	6-311+G(2df,p)	225.3	1390.7	1359.7	265.4
ωB97XD	6-311+G(d,p)	221.3	1391.4	1359.6	277.1
	6-311+G(2df,p)	225.3	1393.8	1361.1	271.0
QCISD	6-311+G(2df,p)	208.3	1386.7	1355.7	265.9
Method	Basis Set	CH ₃ SSeH	CH ₃ SSe [−]		CH ₃ SSe•
		BDE(S–Se)	PA	GPB	HA
B3PW91	6-311+G(d,p)	221.7	1413.2	1382.8	273.8
	6-311+G(2df,p)	233.3	1415.7	1385.5	265.3
ωB97XD	6-311+G(d,p)	219.6	1414.0	1384.2	279.9
	6-311+G(2df,p)	232.5	1417.2	1387.5	270.9
QCISD	6-311+G(2df,p)	218.7	1411.3	1381.1	267.5
Method	Basis Set	CH ₃ SeSH	CH ₃ SeS [−]		CH ₃ SeS•
		BDE(Se–S)	PA	GPB	HA
B3PW91	6-311+G(d,p)	229.4	1435.0	1404.8	287.1
	6-311+G(2df,p)	241.6	1441.7	1411.4	283.6
ωB97XD	6-311+G(d,p)	231.4	1435.6	1405.8	295.6
	6-311+G(2df,p)	245.0	1442.2	1412.4	290.8
QCISD	6-311+G(2df,p)	224.5	1438.9	1408.6	286.1

As for the analogous purely sulfur-containing species (cf. Table 5), the calculated PAs and GPBs of all species obtained using B3PW91 or ωB97XD with either basis set choice gives values within 10 kJ mol^{−1} of the corresponding benchmark values. A similar consistency is observed for the calculated HAs, though with some exceptions. In particular, at the ωB97XD/6-311+G(d,p) level of theory the calculated HAs of CH₂CHSeSe• and CH₃SSe• are 11.2 and 12.4 kJ mol^{−1}, respectively, higher than their corresponding QCISD/6-311+G(2df,p) values. Again, as seen in Table 5, the calculated RX–YH BDEs of all species are generally markedly overestimated by 12.7–26.3 kJ mol^{−1} using either DFT method and basis set. Only three values fall within the desired 10 kJ mol^{−1} error margin and all occur for the mixed chalcogen species; all using the 6-311+G(d,p) basis set.

The thermochemical values provided in Tables 5 and 6 show several key differences between persulfides and perselenides and the mixed chalcogens. These are most clearly and simply illustrated by examination of the calculated benchmark values. In particular, increasing the number of Se atoms in an RX–YH bond reduces its BDE as shown by comparing those of CH₃SSH (236.3 kJ mol^{−1}), CH₃SSeH (218.7 kJ mol^{−1}), CH₃SeSH (223.2 kJ mol^{−1}), and CH₃SeSeH (202.7 kJ mol^{−1}). In addition, a conjugated group adjacent to the RX–XH group increases its BDE slightly by 3–6 kJ mol^{−1}. Meanwhile, the HAs are reasonably consistent and depend primarily on whether the formal radical terminal is a sulfur or selenium. For the former, all values lie within the range 282.7 kJ mol^{−1} (CH₃SS•) to 286.1 kJ mol^{−1} (CH₃SeS•), while the latter are notably lower, between 265.9 kJ mol^{−1} (CH₂CHSeSe•) and 267.3 kJ mol^{−1} (CH₃SeSe• and CH₃SSe•).

Comparison of the PAs and GPBs of these perselenides and mixed per-sulf/selenides with their analogous persulfides (cf. Table 5), shows several interesting trends. It is noted that, for simplicity, as the observed trends were the same for all the DFT methods, the values discussed here refer to those obtained at the benchmark level of theory. Firstly, systematically increasing the occurrence of Se in a per-chalcogenide group decreases their PA and GPB values. For instance, the PAs of CH_3SS^- , CH_3SeS^- , CH_3SSe^- , and CH_3SeSe^- are $1445.4 \text{ kJ mol}^{-1}$, $1438.9 \text{ kJ mol}^{-1}$, $1411.3 \text{ kJ mol}^{-1}$, and $1404.3 \text{ kJ mol}^{-1}$. Simultaneously, their GPB values decrease from $1415.1 \text{ kJ mol}^{-1}$, to $1408.6 \text{ kJ mol}^{-1}$ and $1381.1 \text{ kJ mol}^{-1}$, to $1374.0 \text{ kJ mol}^{-1}$. In addition, replacing CH_3^- with CH_2CH^- decreases the PA and GPB values of the pure persulfides and perselenides by 24–25 and 17–18 kJ mol^{-1} , respectively. This perhaps reflects a larger delocalization when a conjugated group is adjacent and that the effect is less for the selenides.

Extending the persulfides to trisulfides. We also examined the effect of extending the persulfide group by an additional sulfur to a trisulfide; specifically, we considered key bio-relevant thermochemistry of $\text{CH}_3\text{SSS}^\bullet / ^- / \text{H}$ and $\text{CH}_2\text{CHSSS}^\bullet / ^- / \text{H}$. Based on the trends observed for persulfide systems, thermochemical values were obtained using the B3PW91 and ωB97XD DFT methods in combination with the 6-311+G(2df,p) basis set, and again at the QCISD/6-311+G(2df,p) benchmark level of theory (all other data shown in Table S9). As can be seen in Table 7, both DFT methods give thermochemical results in generally good agreement with the benchmark values with B3PW91 slightly preferred, although the differences in average errors are relatively small.

Table 7. Homolytic RS–SH bond dissociation enthalpy (BDE) of RSSSH, proton affinity (PA) and gas-phase basicity (GPB) of RSSS^- , and hydrogen affinity (HA) of RSSS^\bullet (R = CH_3 , CH_2CH). All energies calculated at 298.15K and in kJ mol^{-1} (see Section 3).

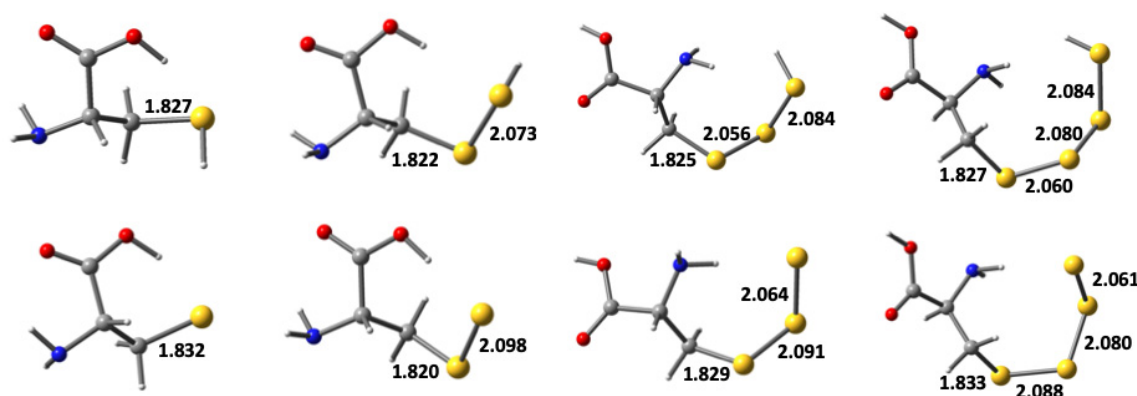
Method	Basis Set	CH_3SSSH	CH_3SSS^-		$\text{CH}_3\text{SSS}^\bullet$
		BDE(RSS–SH)	PA	GPB	HA
B3PW91	6-311+G(2df,p)	193.8	1413.9	1382.4	287.9
ωB97XD	6-311+G(2df,p)	200.4	1415.0	1385.1	297.7
QCISD	6-311+G(2df,p)	183.0	1413.9	1384.1	289.4
		CH_2CHSSSH	$\text{CH}_2\text{CHSSS}^-$		$\text{CH}_2\text{CHSSS}^\bullet$
		BDE(RSS–SH)	PA	GPB	HA
B3PW91	6-311+G(2df,p)	192.8	1399.5	1367.0	290.5
ωB97XD	6-311+G(2df,p)	201.0	1403.0	1370.9	302.0
QCISD	6-311+G(2df,p)	185.7	1403.7	1371.2	295.0

Comparison of the calculated benchmark values of the trisulfides with those of the corresponding persulfides (cf. Table 6) shows that the BDE of $\text{RS}_1\text{S}_2\text{—S}_3\text{H}$ (i.e., the BDE of the terminal $\text{S}_2\text{—S}_3$ bond), where R = CH_3^- and CH_2CH^- , decreases significantly by 53.3 and 56.3 kJ mol^{-1} , respectively. Similarly, their calculated PAs and GPBs decrease markedly by 31–33 and 18–19 kJ mol^{-1} for R = CH_3^- and CH_2CH^- , respectively. As a result of these changes the RSS–SH BDE, and PAs and GPBs of RSSS^- all lie within a narrower range ($\leq 13 \text{ kJ mol}^{-1}$) of each other. This perhaps reflects in part a decrease in the influence of the R group on the increasingly removed S–SH bond. In contrast, the hydrogen affinities of $\text{CH}_3\text{SSS}^\bullet$ and $\text{CH}_2\text{CHSSS}^\bullet$ are 6.7 and 11.5 kJ mol^{-1} higher than that of their corresponding persulfide analogues with values of 289.4 and 295.0 kJ mol^{-1} , respectively.

Cysteine-derived polysulfides: CysSS_nH ($n = 1\text{--}3$). Within biological systems, as noted above, per- and polysulfide derivatives of cysteine play important roles. Hence, we also considered the structures and thermochemistry of such species using the $\omega\text{B97XD}/6\text{-}311\text{G}(2\text{d},\text{p})$ level of theory. This level was selected as it emerged in our earlier study as the most able to provide reliable structures and thermochemistry for related model systems (see above). Selected parameters of optimized structures obtained for CysSS_nH ($n = 0\text{--}3$) and CysSS_n^- ($n = 0\text{--}3$) are provided in Table 8 and representative optimized structures are shown in Figure 1, at this level of theory.

Table 8. Selected optimized bond lengths in ångström (Å) obtained at the ω B97XD/6-311G(2d,p) level of theory for CysSS_nH ($n = 0\text{--}3$) and CysSS_n^- ($n = 0\text{--}3$).

Molecule	C–S ₁	S ₁ –S ₂	S ₂ –S ₃	S ₃ –S ₄
CysSH	1.827			
CysS-SH	1.822	2.073		
CysS-S-SH	1.825	2.056	2.084	
CysS-S-S-SH	1.827	2.060	2.080	2.084
CysS^-	1.832			
CysS-S^-	1.820	2.098		
CysS-S-S^-	1.829	2.091	2.064	
CysS-S-S-S^-	1.833	2.088	2.080	2.061

**Figure 1.** Optimized structures (with C–S and S–S bond lengths given in ångstroms (Å)) obtained at the ω B97XD/6-311G(2d,p) level of theory for neutral cysteine and its polysulfide ($\text{CysS-S}_n\text{H}$ $n = 1\text{--}3$) derivatives (top row), and their corresponding anionic deprotonated derivatives (CysS-S_n^- $n = 0\text{--}3$; bottom row).

As can be seen, for both the neutral and deprotonated derivatives, the $r(\text{C-S})$ bond length decreases slightly upon forming a perthiol/sulfide group, but then gradually lengthens, essentially returning to its length in cysteine, as one goes to the corresponding trithiol/sulfide and tetrathiol/sulfide derivatives. It is also noted that for both CysSSH and CysSS^- , the C–S and S–S bond lengths are in close agreement with the corresponding values obtained at the same level of theory for CH_3SSH (1.816 and 2.067 Å) and CH_3SS^- (1.816 and 2.092 Å), respectively (cf. Table 1). In addition, for the neutral polysulfides the S–S bond in the chain that is farthest removed from the alkyl group has the longest length, with the S–S bonds being sequentially shorter the closer they are to the alkyl group. In contrast, for the corresponding anionic deprotonated series (CysSS_n^- , $n = 0\text{--}3$), the opposite trend is observed; the S–S bond in the chain farthest from the alkyl group is shortest, and they get longer the closer they are to the alkyl group. In the latter species this trend may reflect a diminishing effect of the negative charge on the terminal sulfur atom the further removed the bond.

Thermochemistry of cysteine-derived polysulfides. As for the other species considered above, we calculated the $\text{RS}_n\text{-SH}$ homolytic BDEs for CysSS_nH ($n = 1\text{--}3$), the PAs and GPBs of the CysSS_n^- ($n = 0\text{--}3$) series of derivatives, and the hydrogen affinities (HAs) of the CysSS_n^\bullet ($n = 0\text{--}3$) series of species. However, all values were again only obtained using the chosen ω B97XD/6-311G(2d,p) level of theory. The results obtained are shown in Figure 2A–C.

The calculated $\text{RS}_n\text{-SH}$ ($n = 1\text{--}3$) homolytic bond dissociation enthalpies, that is, the BDE of the terminal S–SH bond in the perthiol chain decreases by 33.7 kJ mol^{−1} from 248.1 to 214.4, upon going from the perthiol ($n = 1$) to trithiol ($n = 2$). It then decreases a further 15.4 kJ mol^{−1} to 199 kJ mol^{−1} upon increasing to the chain further to the tetrathiol ($n = 3$); Figure 2A. This trend suggests that while the strength of the terminal S–SH bond does weaken as the chain is lengthened, it approaches a limiting value below 199.0 kJ mol^{−1}, although possibly not too much lower than that. In contrast,

as seen in Figure 2C, the hydrogen affinities of the $C_{ys}SS_n^\bullet$ ($n = 0-3$) species decrease significantly by 67.8 kJ mol^{-1} upon going from a cysteinyl thiyl radical ($n = 0$; $356.5 \text{ kJ mol}^{-1}$) to the perthiyl radical ($n = 1$; $288.7 \text{ kJ mol}^{-1}$). However, extending the chain further to $n = 2$ or $n = 3$ results in a slight increase in the HAs to $298.7 \text{ kJ mol}^{-1}$ and $295.6 \text{ kJ mol}^{-1}$, respectively. This suggests that at least for HAs of the polysulfur radicals, they are reasonably constant for the perthiyl and beyond.

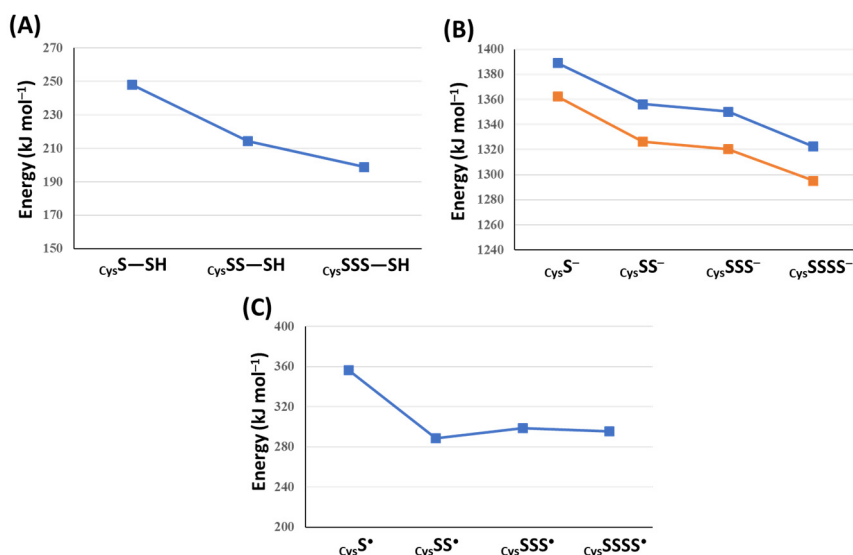


Figure 2. Calculated (at the ω B97XD/6-311G(2d,p) level of theory) values of (A) RS_n-SH BDEs for $C_{ys}SS_nH$ ($n = 1-3$), (B) PAs (blue) and GPBs (orange) of $C_{ys}SS_n^-$ ($n = 0-3$), and (C) HAs of $C_{ys}SS_n^\bullet$ ($n = 0-3$). All energies are in kJ mol^{-1} .

Figure 2B shows that as the polysulfide chain is extended from the cysteine thiolate to $C_{ys}SSSS^-$ both the calculated PAs and GPBs decrease. However, while there are significant decreases of 33.0 (PA) and 35.9 (GPB) kJ mol^{-1} going from the thiolate ($C_{ys}S^-$) to perthiolate ($C_{ys}SS^-$), this does not appear to continue upon extending the chain further. Indeed, extending the chain to $C_{ys}SSS^-$ results in only comparatively small further decreases of 5.8 and 5.9 kJ mol^{-1} to 1350.5 and $1320.6 \text{ kJ mol}^{-1}$. However, upon extending the chain to $C_{ys}SSSS^-$, larger decreases in both the PA and GPB are again observed; they decrease by 27.9 and 25.4 kJ mol^{-1} to 1322.6 and $1295.2 \text{ kJ mol}^{-1}$. This may in part reflect that in the cysteinyl polysulfide derivatives, weak intramolecular hydrogen bonding was observed in some optimized structures between the terminal S^- center and the cysteine's amino group. This interaction would also help decrease PA and GPB values. It should also be noted that comparison of the calculated PAs and GPBs of the cysteine-derived sulfides $C_{ys}SS^-$ and $C_{ys}SSS^-$ with that of their smaller corresponding analogs CH_3SS^- (cf. Table 5) and CH_3SSS^- (cf. Table 7) shows that those of the former two species are markedly lower by $60-90 \text{ kJ mol}^{-1}$. Thus, overall, these results suggest that in biological systems, extending the polysulfide chain will increase its likelihood of being deprotonated and that hydrogen bonding may help to stabilize such anions.

3. Computational Methods

All calculations were performed using the Gaussian 09 [35] and Gaussian 16 [36] suites of programs. Optimized geometries for a systematic series of biologically relevant chemical models, shown in Scheme 2, were obtained using a variety of conventional wavefunction and density functional theory methods applied in conjunction with a range of Pople basis sets from 6-31G(d) to 6-311++G(3df,3pd).

Specifically, the hybrid DFT methods B3LYP and B3PW91, comprised of Becke's three parameter exchange functional [37] (B3) in combination with the Lee, Yang, and Parr correlation functional [38] (LYP) or the Perdew and Wang functional [39] (PW91), were assessed. B3LYP is commonly applied in

the treatment of biomolecular systems while B3PW91 has been used previously for systems containing sulfur and selenium [40,41]. In addition, two *meta*-GGA functionals were assessed; M06-2X [42], a commonly employed functional in the study of enzymatic catalysis, and the more recently developed related functional M08-HX [43]. For this functional, optimized structures were obtained using Gaussian 16 whereas all other structures were obtained with Gaussian 09. Furthermore, the double-hybrid range-corrected functional ω B97XD [44] was also evaluated to further examine any effects of dispersion correction on geometric or energetic parameters. Geometries optimized at these levels of theory were compared to those obtained using the ab initio MP2 (see Supplementary Materials) and QCISD methods. As DFT methods are the preferred choice for biochemical systems due to their computational cost and reliability, the MP2 results are only given in the Table S1 for our baseline geometry assessment of $\text{CH}_3\text{SSH}/^-$ and $\text{CH}_3\text{SeSeH}/^-$. The Minnesota family of functionals (M06-2X and M08-HX) are more empirical and explicitly contain dispersion correction while B3LYP only contains three empirical parameters and has no explicit correction for dispersion.

All optimized structures were confirmed to be minima by harmonic vibrational frequency calculations performed at the same level of theory. These were also used to determine zero-point vibrational energy (ZPVE) and enthalpy corrections for subsequent calculations of a range of their thermochemical properties including proton affinities ($^{298.15\text{K}}\text{PA}_{\text{A}^-} = -\text{H} = -(\text{H}_{\text{AH}} - \text{H}_{\text{A}^-} - \text{H}_{\text{H}^+})$), gas-phase basicities ($^{298.15\text{K}}\text{GPB}_{\text{A}^-} = -\text{G} = -(\text{PA} - \text{T}(\text{S}_{\text{AH}} - \text{S}_{\text{A}^-} - \text{S}_{\text{H}^+}))$), and hydrogen affinities ($^{298.15\text{K}}\text{HA}_{\text{A}} = -\text{H} = -(\text{H}_{\text{AH}} - \text{H}_{\text{A}} - \text{H}_{\text{H}})$) [45,46]. In addition, homolytic bond dissociation enthalpies were calculated for production of the $\cdot\text{SH}$ or $\cdot\text{SeH}$ radicals ($^{298.15\text{K}}\text{BDE}_{\text{AX-XH}} = \text{H} = \text{H}_{\text{AX}\cdot} + \text{H}_{\text{XH}\cdot} - \text{H}_{\text{AXXH}}$).

4. Conclusions

The reliability and accuracy of several commonly used DFT functionals (e.g., B3LYP, B3PW91, ω B97XD, M06-2X, M08-HX) as well as MP2 was assessed for a systematic series of bio-relevant polysulfur/selenium-containing systems. In particular, optimized structures and thermodynamic properties of a range of $\text{RX}_n(\text{H})$ ($\text{X} = \text{S}, \text{Se}$, $\text{R} = \text{CH}_3, \text{CH}_2\text{CH}$, and cysteine, $n = 1-4$) were examined with a variety of Pople basis sets of increasing size. We offer the following conclusions from this detailed study:

1. Evaluation of the bond lengths in $\text{CH}_3\text{XXH}/^-$ ($\text{X} = \text{S}, \text{Se}$, cf. Table 1) showed that the S–S bond is the most sensitive to changes in basis set. The smallest basis set used (6-31G(d)) frequently resulted in optimized geometries that were very similar to the benchmark given by QCISD/6-311+G(2df,p), although the preferred basis sets were 6-311G(2d,p) and 6-311G(df,p) due to the higher sensitivity of sulfur to basis set choice.
2. We also saw that M08-HX did not offer much improvement over M06-2X and in some cases was detrimental. The best functionals for geometry optimization were found to be B3PW91, ω B97XD and M06-2X.
3. In the conjugated system CH_2CHXXH , the C–X bond length decreases due to more delocalized electron density.
4. In mixed chalcogen species, the location of the chalcogen atom has a significant effect on the X–Y bond length. The RSe-S^- bond is slightly longer than the RS-Se^- bond since sulfur takes on more negative charge. Deprotonation of polysulfide species increases the C–S bond as well, for the same reason: charge delocalization along a sulfur chain.
5. In the polysulfide species PA, GPB, BDE, and HA all decrease with the increasing sulfur chain. The lower PA and GPB values indicate that in a biological system, polysulfide chains are more likely to exist as deprotonated rather than neutral species compared to the parent thiol or selenol.
6. To perform reliable thermochemical calculations, the ω B97XD/6-311G(2d,p) level of theory was found to give the most accurate results relative to the benchmark and this was then used to evaluate the geometry and thermochemistry of the more complex cysteine and cysteine per/polysulfide species.

Supplementary Materials: Tables of selected optimized bond lengths obtained (i) at the MP2 level of theory for CH_3XXH and CH_3XX^- ($\text{X} = \text{S}, \text{Se}$); and using several DFT functionals for (ii) CH_2CHSSH and CH_2CHSS^- , and $\text{CH}_2\text{CHSeSeH}$ and $\text{CH}_2\text{CHSeSe}^-$; (iii) CH_3XYH and CH_3XY^- ($\text{X} = \text{S}, \text{Se}$; $\text{Y} = \text{Se}, \text{S}$); (iv) $\text{RSSSH}/^-$ ($\text{R} = \text{CH}_3, \text{CH}_2\text{CH}$). Table summarizing Mulliken charges on each sulfur atom in $\text{RSSSH}/^-$ ($\text{R} = \text{CH}_3, \text{CH}_2\text{CH}$) as obtained at several selected levels of theory. Tables of homolytic S–S bond dissociation enthalpy (BDE) of RXYH , proton affinity (PA) and gas-phase basicity (GPB) of RXY^- , and hydrogen affinity (HA) of RXY^\bullet ($\text{R} = \text{CH}_3, \text{CH}_2\text{CH}$; $\text{X} = \text{S}, \text{Se}$ / $\text{Y} = \text{S}, \text{Se}$). Table of Homolytic S–S bond dissociation enthalpy (BDE) of RSSSH , proton affinity (PA) and gas-phase basicity (GPB) of RSSS^- , and hydrogen affinity (HA) of RSSS^\bullet ($\text{R} = \text{CH}_3, \text{CH}_2\text{CH}$). Gaussian archive entry for each molecule considered in this present study.

Author Contributions: Conceptualization, J.G.; Data curation, S.N., P.M. and J.G.; Formal analysis, S.N., P.M., J.H. and J.G.; Funding acquisition, J.G.; Investigation, S.N., P.M. and J.G.; Methodology, J.G.; Project administration, J.G.; Resources, J.G.; Supervision, J.G.; Validation, J.G.; Visualization, S.N., P.M. and J.G.; Writing—original draft, S.N., P.M., J.H. and J.G.; Writing—review & editing, S.N., P.M., J.H. and J.G. The manuscript was written through the contributions of all authors. All authors have given approval to the final version of the manuscript.

Funding: We acknowledge the Natural Science and Engineering Research Council of Canada (NSERC) for financial support. S.N. acknowledges support from an Ontario Trillium Scholarship. P.J.M. acknowledges support from an NSERC Master’s Canada Graduate Scholarship.

Acknowledgments: We acknowledge Compute Canada and SHARCNET for additional computational resources.

Conflicts of Interest: The authors declare no conflict of interest. The funders had no role in the design of the study; in the collection, analyses, or interpretation of data; in the writing of the manuscript, and in the decision to publish the results.

References

1. Zhong, L.W.; Holmgren, A. Essential role of selenium in the catalytic activities of mammalian thioredoxin reductase revealed by characterization of recombinant enzymes with selenocysteine mutations. *J. Biol. Chem.* **2000**, *275*, 18121–18128. [[CrossRef](#)] [[PubMed](#)]
2. Fernandez, F.J.; Arda, A.; Lopez-Esteva, M.; Aranda, J.; Pena-Soler, E.; Garces, F.; Round, A.; Campos-Olivas, R.; Bruix, M.; Coll, M.; et al. Mechanism of Sulfur Transfer Across Protein-Protein Interfaces: The Cysteine Desulfurase Model System. *ACS Catal.* **2016**, *6*, 3975–3984. [[CrossRef](#)]
3. Kahya, M.C.; Naziroglu, M.; Ovey, I.S. Modulation of Diabetes-Induced Oxidative Stress, Apoptosis, and Ca^{2+} Entry Through TRPM2 and TRPV1 Channels in Dorsal Root Ganglion and Hippocampus of Diabetic Rats by Melatonin and Selenium. *Mol. Neurobiol.* **2017**, *54*, 2345–2360. [[CrossRef](#)] [[PubMed](#)]
4. Paulsen, C.E.; Carroll, K.S. Cysteine-mediated redox signaling: Chemistry, biology, and tools for discovery. *Chem. Rev.* **2013**, *113*, 4633–4679. [[CrossRef](#)] [[PubMed](#)]
5. Garcia-Santamarina, S.; Boronat, S.; Hidalgo, E. Reversible Cysteine Oxidation in Hydrogen Peroxide Sensing and Signal Transduction. *Biochemistry* **2014**, *53*, 2560–2580. [[CrossRef](#)]
6. Huang, Z.; Rose, A.H.; Hoffmann, P.R. The role of selenium in inflammation and immunity: From molecular mechanisms to therapeutic opportunities. *Antioxid. Redox. Signal.* **2012**, *16*, 705–743. [[CrossRef](#)] [[PubMed](#)]
7. Ida, T.; Sawa, T.; Ihara, H.; Tsuchiya, Y.; Watanabe, Y.; Kumagai, Y.; Suematsu, M.; Motohashi, H.; Fujii, S.; Matsunaga, T.; et al. Reactive cysteine persulfides and S-polythiolation regulate oxidative stress and redox signaling. *Proc. Natl. Acad. Sci. USA* **2014**, *111*, 7606–7611. [[CrossRef](#)]
8. Kim, H.J.; Ha, S.; Lee, H.Y.; Lee, K.J. ROSics: Chemistry and proteomics of cysteine modifications in redox biology. *Mass Spectrom. Rev.* **2015**, *34*, 184–208. [[CrossRef](#)]
9. Jacobs, E.T.; Jiang, R.; Alberts, D.S.; Greenberg, E.R.; Gunter, E.W.; Karagas, M.R.; Lanza, E.; Ratnasinghe, L.; Reid, M.E.; Schatzkin, A.; et al. Selenium and colorectal adenoma: Results of a pooled analysis. *J. Natl. Cancer Inst.* **2004**, *96*, 1669–1675. [[CrossRef](#)]
10. Wu, G.; Fang, Y.Z.; Yang, S.; Lupton, J.R.; Turner, N.D. Glutathione metabolism and its implications for health. *J. Nutr.* **2004**, *134*, 489–492. [[CrossRef](#)]
11. Giles, G.I.; Tasker, K.M.; Jacob, C. Hypothesis: The role of reactive sulfur species in oxidative stress. *Free Radic. Biol. Med.* **2001**, *31*, 1279–1283. [[CrossRef](#)]
12. Toohey, J.I. Sulfur signaling: Is the agent sulfide or sulfane? *Anal. Biochem.* **2011**, *413*, 1–7. [[CrossRef](#)] [[PubMed](#)]
13. Kimura, H. Physiological role of hydrogen sulfide and polysulfide in the central nervous system. *Neurochem. Int.* **2013**, *63*, 492–497. [[CrossRef](#)] [[PubMed](#)]

14. Kaneko, Y.; Kimura, Y.; Kimura, H.; Niki, I. L-cysteine inhibits insulin release from the pancreatic beta-cell—Possible involvement of metabolic production of hydrogen sulfide, a novel gasotransmitter. *Diabetes* **2006**, *55*, 1391–1397. [[CrossRef](#)] [[PubMed](#)]
15. Lo Faro, M.L.; Fox, B.; Whatmore, J.L.; Winyard, P.G.; Whiteman, M. Hydrogen sulfide and nitric oxide interactions in inflammation. *Nitric Oxide Biol. Chem.* **2014**, *41*, 38–47. [[CrossRef](#)] [[PubMed](#)]
16. Yu, B.; Zheng, Y.; Yuan, Z.; Li, S.; Zhu, H.; De La Cruz, L.K.; Zhang, J.; Ji, K.; Wang, S.; Wang, B. Toward Direct Protein S-Persulfidation: A Prodrug Approach That Directly Delivers Hydrogen Persulfide. *J. Am. Chem. Soc.* **2018**, *140*, 30–33. [[CrossRef](#)]
17. Giles, G.I.; Nasim, M.J.; Ali, W.; Jacob, C. The Reactive Sulfur Species Concept: 15 Years On. *Antioxidants* **2017**, *6*, 38. [[CrossRef](#)] [[PubMed](#)]
18. Shen, X.G.; Peter, E.A.; Bir, S.; Wang, R.; Kevil, C.G. Analytical measurement of discrete hydrogen sulfide pools in biological specimens. *Free Radic. Biol. Med.* **2012**, *52*, 2276–2283. [[CrossRef](#)]
19. Iciek, M.; Wlodek, L. Biosynthesis and biological properties of compounds containing highly reactive, reduced sulfane sulfur. *Polish J. Pharmacol.* **2001**, *53*, 215–225.
20. Mishanina, A.V.; Libiad, M.; Banerjee, R. Biogenesis of reactive sulfur species for signaling by hydrogen sulfide oxidation pathways. *Nat. Chem. Biol.* **2015**, *11*, 457–464. [[CrossRef](#)]
21. Akaike, T.; Ida, T.; Wei, F.Y.; Nishida, M.; Kumagai, Y.; Alam, M.M.; Ihara, H.; Sawa, T.; Matsunaga, T.; Kasamatsu, S.; et al. Cysteinyl-tRNA synthetase governs cysteine polysulfidation and mitochondrial bioenergetics. *Nat. Commun.* **2017**, *8*, 1177. [[CrossRef](#)] [[PubMed](#)]
22. Koike, S.; Nishimoto, S.; Ogasawara, Y. Cysteine persulfides and polysulfides produced by exchange reactions with H₂S protect SH-SY5Y cells from methylglyoxal-induced toxicity through Nrf2 activation. *Redox Biol.* **2017**, *12*, 530–539. [[CrossRef](#)] [[PubMed](#)]
23. Munchberg, U.; Anwar, A.; Mecklenburg, S.; Jacob, C. Polysulfides as biologically active ingredients of garlic. *Org. Biomol. Chem.* **2007**, *5*, 1505–1518. [[CrossRef](#)] [[PubMed](#)]
24. Gruhlke, M.C.H.; Nicco, C.; Batteux, F.; Slusarenko, A.J. The Effects of Allicin, a Reactive Sulfur Species from Garlic, on a Selection of Mammalian Cell Lines. *Antioxidants* **2017**, *6*, 1. [[CrossRef](#)]
25. Millikin, R.; Bianco, C.L.; White, C.; Saund, S.S.; Henriquez, S.; Sosa, V.; Akaike, T.; Kumagai, Y.; Soeda, S.; Toscano, J.P.; et al. The chemical biology of protein hydropersulfides: Studies of a possible protective function of biological hydropersulfide generation. *Free Radic. Biol. Med.* **2016**, *97*, 136–147. [[CrossRef](#)] [[PubMed](#)]
26. Cerqueira, N.M.; Fernandes, P.A.; Gonzalez, P.J.; Moura, J.J.; Ramos, M.J. The sulfur shift: An activation mechanism for periplasmic nitrate reductase and formate dehydrogenase. *Inorg. Chem.* **2013**, *52*, 10766–10772. [[CrossRef](#)] [[PubMed](#)]
27. Cheng, Q.; Sandalova, T.; Lindqvist, Y.; Arner, E.S. Crystal structure and catalysis of the selenoprotein thioredoxin reductase 1. *J. Biol. Chem.* **2009**, *284*, 3998–4008. [[CrossRef](#)] [[PubMed](#)]
28. Searle, P.A.; Molinski, T.F. 5 New Alkaloids from the Tropical Ascidian, *Lissoclinum* Sp—Lissoclinotoxin-a is Chiral. *J. Org. Chem.* **1994**, *59*, 6600–6605. [[CrossRef](#)]
29. Brzostowska, E.M.; Greer, A. The role of amine in the mechanism of pentathiepin (polysulfur) antitumor agents. *J. Am. Chem. Soc.* **2003**, *125*, 396–404. [[CrossRef](#)]
30. Chauvin, J.P.R.; Griesser, M.; Pratt, D.A. Hydropersulfides: H-Atom Transfer Agents Par Excellence. *J. Am. Chem. Soc.* **2017**, *139*, 6484–6493. [[CrossRef](#)]
31. Bortoli, M.; Torsello, M.; Bickelhaupt, F.M.; Orian, L. Role of the Chalcogen (S, Se, Te) in the Oxidation Mechanism of the Glutathione Peroxidase Active Site. *Chem. Phys. Chem.* **2017**, *18*, 2990–2998. [[CrossRef](#)] [[PubMed](#)]
32. Bachrach, S.M.; Demoin, D.W.; Luk, M.; Miller, J.V. Nucleophilic attack at selenium in diselenides and selenosulfides. A computational study. *J. Phys. Chem. A* **2004**, *108*, 4040–4046. [[CrossRef](#)]
33. Huang, G.T.; Yu, J.S.K. Enzyme Catalysis that Paves the Way for S-Sulphydration via Sulfur Atom Transfer. *J. Phys. Chem. B* **2016**, *120*, 4608–4615. [[CrossRef](#)] [[PubMed](#)]
34. Koch, W.; Holthausen, M.C. *A Chemist's Guide to Density Functional Theory*, 2nd ed.; Wiley-VCH: Weinheim, Germany; New York, NY, USA, 2001.
35. Frisch, M.J.; Trucks, G.W.; Schlegel, H.B.; Scuseria, G.E.; Robb, M.A.; Cheeseman, J.R.; Scalmani, G.; Barone, V.; Petersson, G.A.; Nakatsuji, H.; et al. *Gaussian 09, E.01*; Gaussian Inc.: Wallingford, CT, USA, 2013.
36. Frisch, M.J.; Trucks, G.W.; Schlegel, H.B.; Scuseria, G.E.; Robb, M.A.; Scalmani, G.; Barone, V.; Petersson, G.A.; Li, X.; Caricato, M.; et al. *Gaussian 16*; Gaussian Inc.: Wallingford, CT, USA, 2016.

37. Becke, A.D. A New Mixing of Hartree-Fock and Local Density-Functional Theories. *J. Chem. Phys.* **1993**, *98*, 1372–1377. [[CrossRef](#)]
38. Lee, C.T.; Yang, W.T.; Parr, R.G. Development of the Colle-Salvetti Correlation-Energy Formula into a Functional of the Electron-Density. *Phys. Rev. B* **1988**, *37*, 785–789. [[CrossRef](#)]
39. Perdew, J.P.; Wang, Y. Accurate and Simple Analytic Representation of the Electron-Gas Correlation-Energy. *Phys. Rev. B* **1992**, *45*, 13244–13249. [[CrossRef](#)]
40. Jursic, B.S. Density functional theory and complete basis set ab initio evaluation of proton affinity for some selected chemical systems. *J. Mol. Struct. Theochem* **1999**, *487*, 193–203. [[CrossRef](#)]
41. Bras, N.F.; Perez, M.A.S.; Fernandes, P.A.; Silva, P.J.; Ramos, M.J. Accuracy of Density Functionals in the Prediction of Electronic Proton Affinities of Amino Acid Side Chains. *J. Chem. Theory Comput.* **2011**, *7*, 3898–3908. [[CrossRef](#)]
42. Zhao, Y.; Truhlar, D.G. The M06 suite of density functionals for main group thermochemistry, thermochemical kinetics, noncovalent interactions, excited states, and transition elements: Two new functionals and systematic testing of four M06-class functionals and 12 other functionals. *Theor. Chem. Acc.* **2008**, *120*, 215–241.
43. Zhao, Y.; Truhlar, D.G. Exploring the Limit of Accuracy of the Global Hybrid Meta Density Functional for Main-Group Thermochemistry, Kinetics, and Noncovalent Interactions. *J. Chem. Theory Comput.* **2008**, *4*, 1849–1868. [[CrossRef](#)]
44. Chai, J.D.; Head-Gordon, M. Long-range corrected hybrid density functionals with damped atom-atom dispersion corrections. *Phys. Chem. Chem. Phys.* **2008**, *10*, 6615–6620. [[CrossRef](#)] [[PubMed](#)]
45. Hunter, E.P.L.; Lias, S.G. Evaluated gas phase basicities and proton affinities of molecules: An update. *J. Phys. Chem. Ref. Data* **1998**, *27*, 413–656. [[CrossRef](#)]
46. Moser, A.; Range, K.; York, D.M. Accurate Proton Affinity and Gas-Phase Basicity Values for Molecules Important in Biocatalysis. *J. Phys. Chem. B* **2010**, *114*, 13911–13921. [[CrossRef](#)] [[PubMed](#)]



© 2018 by the authors. Licensee MDPI, Basel, Switzerland. This article is an open access article distributed under the terms and conditions of the Creative Commons Attribution (CC BY) license (<http://creativecommons.org/licenses/by/4.0/>).